THERMAL WAVE PHYSICS IN NDE

Allan Rosencwaig

Therma-Wave, Inc.

Fremont, CA 94539

INTRODUCTION

There has been considerable interest lately in imaging techniques that employ thermal waves [1-4]. In thermal-wave imaging, a beam of energy, usually a laser or electron beam, is focused and scanned across the surface of a sample. This beam is generally intensity-modulated at a frequency in the range of 10kHz to 10MHz. As the beam scans across the sample it is absorbed at or near the surface, and periodic surface heating results at the beam modulation frequency. This periodic heating is the source of thermal waves, which propagate from the heated region. The thermal waves are diffusive waves similar to eddy current waves, evanescent waves, and other critically damped phenomena that travel only one to two wavelengths before their intensity becomes negligibly small. Nevertheless, within their range, the thermal waves interact with thermal features in a manner that is mathematically similar to the scattering and reflection processes of conventional propagating waves [5]. Thus any features on or beneath the surface of the sample that are within the range of these thermal waves and that have thermal characteristics different from their surroundings will reflect and scatter the waves and thus become visible.

These thermal features can be defined as those regions of an otherwise homogeneous material that exhibit variations, relative to their surroundings, in either the thermal conductivity κ, the volume specific heat ρC, and in some instances the thermal expansion coefficient α. Variations in these thermal parameters arise, most commonly, from variations in the local lattice structure of the material, and, for metals and other good electrical conductors, from variations in the local carrier concentration as well.

METHODOLOGY

Imaging of these thermal features requires detection of the scattered and reflected thermal waves. This detection is currently accomplished by several different techniques.

However, thermal-wave imaging at the high spatial resolution needed for microelectronics investigations, where micron-sized features must be resolved, requires the detection of high frequency (MHz range) thermal waves. To date only the thermoacoustic detection method has been used routinely for detecting such high frequency thermal waves [1, 6].

Thermoacoustic signals occur in any sample with a non-zero thermal expansion coefficient because of the periodic stress-strain conditions in the heated volume defined by the thermal waves. Thus, 1-MHz thermal waves give rise to 1-MHz acoustic waves. These thermoacoustic waves are propagating waves of much longer wavelengths, typically a few millimeters at 1MHz, compared to a few microns for thermal waves at the same frequency. The magnitude and phase of the thermoacoustic waves are directly related to the temperature profiles in the heated volume and thus are directly affected by the presence of scattered and reflected thermal-waves.

Thermoacoustically generated ultrasonic waves were predicted by White [7] and first used for imaging by von Gutfeld and Melcher [8]. These and subsequent experiments were concerned, however, with the use of thermoacoustic waves for ultrasonic imaging, where the interactions of the acoustic waves with the elastic features in the sample produce the principal contrast mechanisms. The possibility of using the thermal waves, which precede the thermoacoustic waves for the imaging of thermal features was not realized at the time. Although acoustic waves are detected, thermal-wave imaging with the thermoacoustic probe is not acoustic imaging, since the acoustic waves always have wavelengths many orders of magnitude greater than the thermal waves and thus are not able to image the same small features. That is, the acoustic waves simply carry or amplify the information describing the thermal-wave event. In thermal-wave imaging, the thermoacoustic waves are thus used as a monitor to detect the presence of thermal waves scattered or reflected from thermal features.

Most high-frequency thermal-wave imaging is performed in a scanning electron microscope, SEM, where an intensity-modulated electron beam is used to generate the thermal waves. The experiments that will be reported here all have been performed with a Therma-Wave, Inc. Model 101 system attached to a Hitachi S-520 scanning electron microscope which is described elsewhere [10]. With this system, we have performed high-resolution, thermal-wave imaging on many different materials. We have detected and imaged subsurface mechanical defects such as microcracks and voids, grain boundaries, grains, and dislocations, and dopant regions and lattice variations in crystals.

SPECIFIC APPLICATIONS

Subsurface Mechanical Defects

Subsurface mechanical defects such as voids, cracks and delaminations represent substantial thermal features and thus are readily detected with a thermal-wave microscope [1, 9, 10]. One illustration of this application is shown

in Figure 1. Figure 1a is the electron image of a Si device. The thermal-wave image in Figure 1b shows a large subsurface crack network in the Si chip and a delamination or subsurface chip-out region at the top in the center. Neither of these mechanical defects is visible with either optical or electron microscopy. Other examples of thermal-wave imaging of subsurface mechanical defects have been presented elsewhere [9, 10].

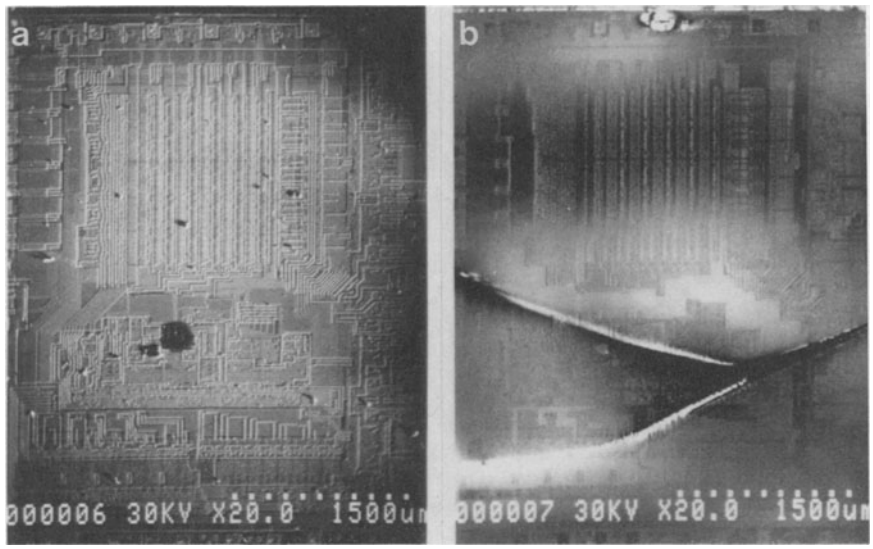

Figure 1: Examples of subsurface mechanical defects in a Si device. The electron micrograph (a) shows no defect features. The thermal-wave image (b) shows a subsurface network of microcracks in the lower half of the device and a subsurface delamination or chip-out in the top center.

Metallography

Thermal waves can be used to image variations in single and multi-phase crystals. This ability is of considerable utility in metallography, since different metallic phases or grains can be readily imaged with no special sample preparation. We illustrate this in Figure 2 where the columnar or dendritic grains and the various transition and precipitation zones are clearly visible in the thermal-wave image of a weld region in a Co-Cr alloy. In addition, we can see in the thermal-wave image, a crack forming along the sharp precipitation zone in the center of the dendritic grains. This image dramatically reveals that we are dealing with an inherently weak weld due to the presence of the large dendritic grains and the sharp transition or precipitation zone. In addition, the thermal-wave image shows that this weld already has an incipient crack forming in it along the precipitation zone. Such images cannot be obtained by any other nondestructive means.

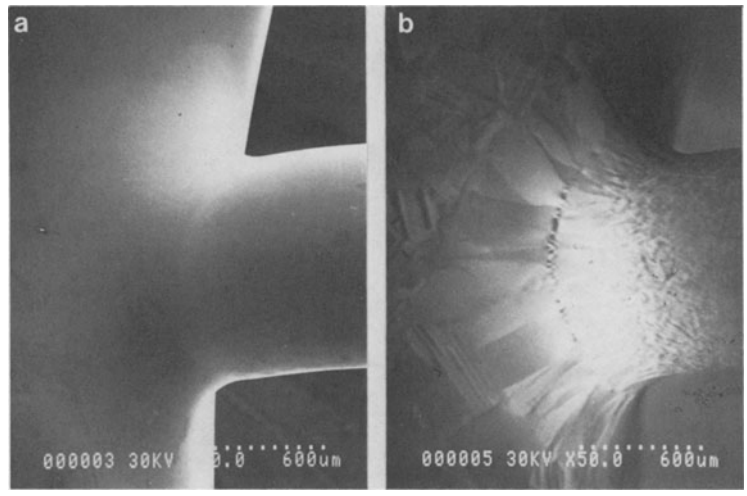

Figure 2: a.) Electron micrograph of a polished weld region in a Co-Cr alloy. b.) Thermal-wave micrograph of same region showing all of the grain microstructure including the dendritic grains and transition zones in the weld region. Note the presence of a subsurface microcrack forming along the sharp precipitation zone near the center of the weld.

Another example is shown in Figure 3 which shows the electron and thermal-wave images of an Al-Zn alloy. The electron image (a) shows only topographical features, while the thermal-wave image (b) clearly shows both the grain structure and the presence of Fe or Sn precipitates.

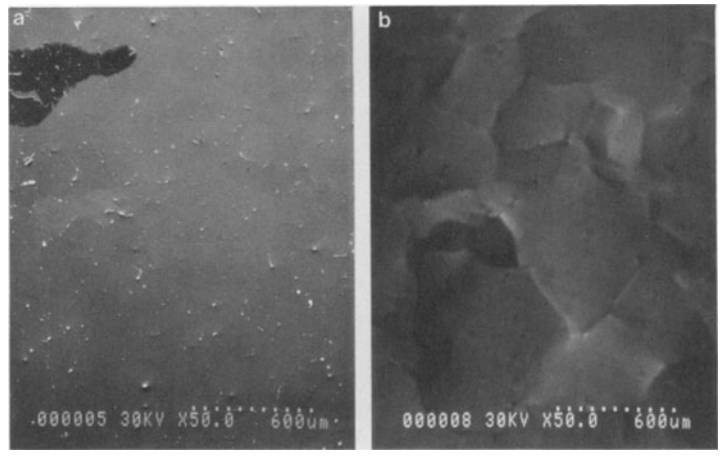

Figure 3: Electron (a) and thermal-wave (b) micrographs of an Al-Zn alloy. The thermal-wave micrograph shows the Al-Zn grains, and the presence of Fe or Sn precipitates.

As seen from the above Figures, and from those obtained by other investigators [2, 11], grain structures in single and multi-phase metals and alloys show up very clearly in thermal-wave images. It should be kept in mind that conventional SEM images will usually show grain contrast only for multi-phase materials with substantial atomic number differ-

differences between grains, and for single-phase materials only if they have been previously etched or if one can perform electron channeling experiments.

Crystalline Disruptions and Variations

When a crystal lattice is highly ordered, minor changes in lattice structure can produce measurable changes in the local thermal conductivity of the material and thus can be imaged with a thermal-wave microscope [10, 12]. This capability is illustrated in Figure 4 which shows a GaAs device. The optical and electron micrographs image the visible features of the gate structures in the devices. The thermal-wave image shows, in addition, the Si-doped regions of the GaAs, since these regions have a different thermal conductivity than the undoped regions. Such images permit a rapid and nondestructive analysis of the effects of lateral diffusion of dopant in semi-conducting crystals.

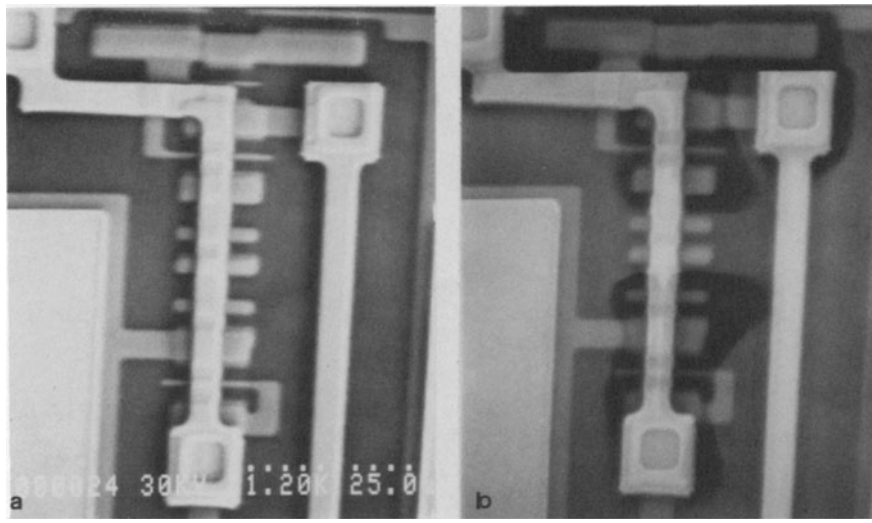

Figure 4: Images of a GaAs device. The electron micrograph (a) shows the surface circuit features. The thermal-wave image (b) shows, in addition, the Si-doped regions around and underneath some of the circuit structures.

Correlations with EBIC and XRT

Thermal features that arise either from mechanical defects or from metallic grains and grain boundaries are usually easy to recognize. However, thermal features arising from more subtle crystalline disruptions and variations, such as those just described are more difficult to identify. Before thermal-wave microscopy can be accepted as a routine, standard analytical technique, one needs to establish a direct correlation of some of these less obvious thermal-wave images with those obtained with other more widely accepted techniques. Below, we discuss two such correlations, one with electron beam induced current (EBIC) and the other with x-ray topography (XRT).

EBIC analysis is an important tool for characterizing electrically active features in semiconductors [13]. The

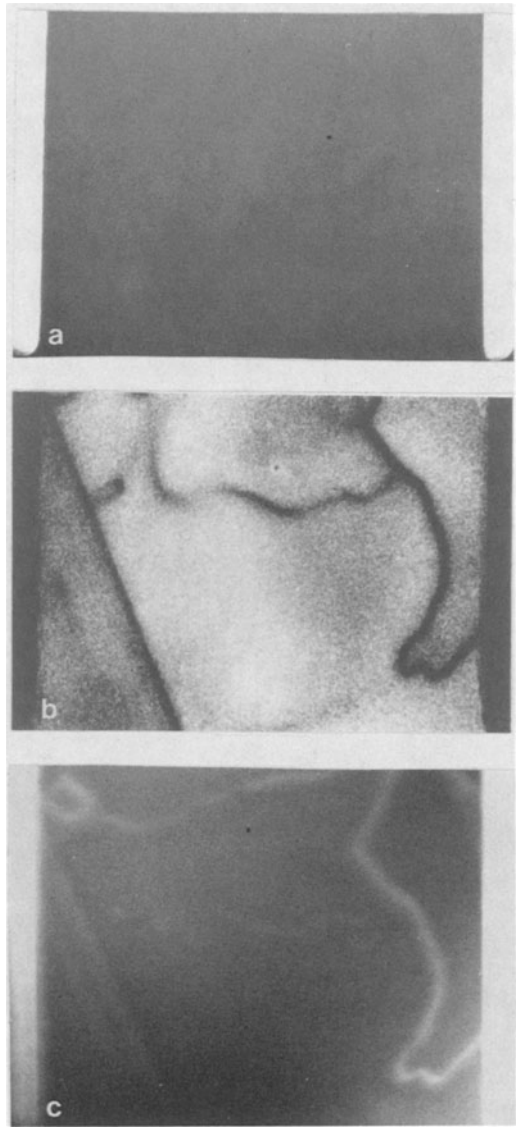

Figure 5: a.) Electron micrograph of a single grain region of Si solar cell material. b.) EBIC image of same region showing the sub-grain boundries that affect the electron-hole current in the p-n junction. c.) Thermal-wave image of same region showing the same features as the EBIC image.

correlation study between EBIC and thermal-wave imaging was performed with Si solar cell material. This is large-grain ribbon material which has been polished to produce a smooth surface for the EBIC studies. Figure 5a is an electron image of a small area of the sample, in which the only features seen are the contact metallization lines from the solar cell. Figure 5b is the EBIC picture of the same area showing detail due to subgrain boundaries. The thermal-wave image in Figure 5c shows all the same subgrain boundary features as the EBIC micrograph with similar resolution. This suggests that thermal-wave microscopy can be used to study

the same features that EBIC would show, but without the need to make the p-n junctions required for EBIC studies.

X-ray topography is a technique which uses x-ray diffraction to image features which produce diffraction contrast, [14] (i.e., produce changes in diffracted beam angles). Thus it is applied primarily to single crystal or, at least, highly oriented polycrystalline samples. Contrast is produced at crystalline defects such as dislocations, twins, or stacking faults which are regions of high strain and often the location of precipitate particles.

Figure 6 is a part of a reflection topograph taken on an LEC-grown GaAs crystal. A 30-hour exposure was required to obtain this image. The patterns seen in this topograph are primarily very dense dislocation networks.

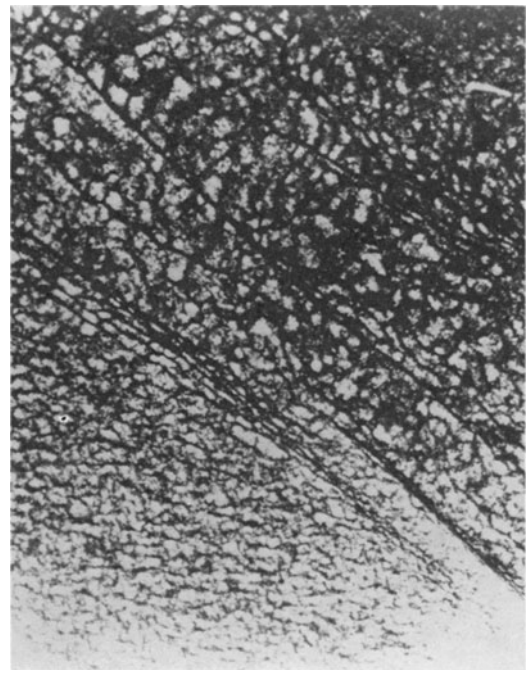

Figure 6: a.) X-ray topograph (XRT) of a section of LEC-grown GaAs crystal showing a dense network of dislocations.

For comparison, Figure 7 is a thermal-wave micrograph of the same area of the crystal. Clearly, the same features are visible in the two imaging techniques and, in fact the dislocation networks appear to be somewhat better resolved in the thermal-wave image. However, whereas the x-ray topograph required 30 hours to obtain, the thermal-wave image was obtained in two minutes. We have also seen features at higher magnification with thermal-wave imaging which are probably images of small dislocation clusters.

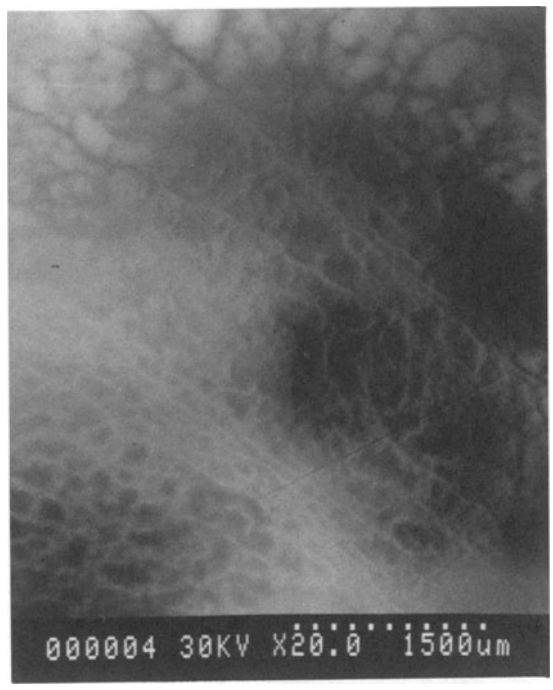

Figure 7: Thermal-wave image of same region of LEC-grown GaAs crystal shown in Fig. 6. The same dense network of dislocations is visible. Note the crack that appears in both Figures in the lower right-hand corner.

The contrast mechanism in the XRT micrograph is clearly the variations in the local elastic strain. That the elastic strain variations are not the direct contrast mechanism for the thermal-wave micrograph can be deduced both from theoretical arguments and from recent work related to acoustic microscopy [15, 16]. This work has shown, both experimentally and theoretically, that dislocations in semiconducting crystals are not detectable by even the micronsized ultrasonic waves generated in a high-frequency acoustic microscope, because the dislocation strain fields produce negligible variations in the local elastic constants. Thus the thermal-wave contrast mechanism must be attributable primarily to variations in the local thermal conductivity, which, being a dynamic transport property, is more sensitive to lattice perturbations than are the static elastic properties.

Thermal-wave imaging thus appears to be as powerful a technique as x-ray topography for imaging dislocations in GaAs materials, but is much faster and simpler.

CONCLUSIONS

Thermal-wave imaging is a means of detecting and imaging previously invisible thermal features. Its applications in materials analysis are many and diverse. These include the

detection and imaging of subsurface defects, including interfacial flaws and microcracks; the detection and characterization of areas of a crystalline lattice that have been modified through the introduction of foreign ions or defects; and the imaging of dislocations both in clusters and in networks. In addition, the ability to image crystalline phases and grains in single and multi-phase materials with no special sample preparation makes possible more convenient, nondestructive in-situ, and perhaps even dynamic studies of metals, composites, and other materials. In biology, the method may be used in the future to analyze and map the microscopic structure of membranes and cells in terms of their local thermal parameters, thereby providing potentially valuable data.

REFERENCES

1. A. Rosencwaig, Science 218, 223 (1982).
2. G.S. Cargill, Physics Today 34, 27 (1981).
3. G. Busse, In Scanned Image Microscopy, ed. E.A. Ash, (Academic Press, London/New York, 1980) pp. 341-345.
4. R.L. Thomas, L.D. Favro, K.R. Grice, L.J. Inglehart, P.K. Kuo, J. Lhota and G. Busse, Proc. 1982 Ultrasonics Symposium, ed. B.R. McAvoy, (IEEE Press, New York, 1982) pp. 586-590.
5. J. Opsal and A. Rosencwaig, J. Appl. Phys. 53, 4240 (1982).
6. A. Rosencwaig and G. Busse, Appl. Phys. Lett. 36, 725 (1980).
7. R.M. White, J. Appl. Phys. 34, 3559 (1963).
8. R.J. von Gutfeld, and R.L. Melcher, Appl. Phys. Lett. 33, 257 (1977).
9. E. Brandis and A. Rosencwaig, Appl. Phys. Lett. 37, 98 (1980).
10. A. Rosencwaig, In VLSI Electronics: Microstructure Science, vol. 9, ed. N.G. Einspruch, (Academic Press, New York, 1985) pp. 227-288.
11. D.G. Davies, Scanning Electron Microscopy III/1983, 1163 (1983).
12. A. Rosencwaig and R.M. White, Appl. Phys. Lett. 38, 165 (1981).
13. K.V. Ravi, C.J. Varker and C.E. Volk, J. Electrochem. Soc. 120, 533 (1973).
14. B.K. Tanner and D.K. Bowen, Characterization of Crystal Growth Defects by X-ray Methods, (Plenum Press, New York, 1980).
15. P.E. Sulewski, R.D. Dynes, S. Mahajan and D.J. Bishop, J. Appl. Phys. 54, 5711 (1983).
16. P.E. Sulewski and D.J. Bishop, J. Appl. Phys. 54, 5715 (1983).

DISCUSSION

Mr. William J. Baxter (General Motors): When you show us high-resolution pictures so we can see dislocations and grain structure, how thin does the specimen have to be?

Mr. Opsal: Some of those, the stainless steel samples, for example, could be a few millimeters thick.

There's a problem in this kind of a detection scheme, which is collecting the thermo-elastic response to the sample. If the samples are too thick, then we don't seem to have the sensitivity that we should have that we would like, so we are often better off making the samples thinner, but they don't have to be thinner than more than 2 or 3 millimeters.

Mr. David Cheeke (Sherbrooke): I wonder if you could tell me what your sensitivity is to the variation in doping levels. Can you just distinguish between doped and undoped, or can you look at fine variations?

Mr. Opsal: Well, in a different kind of measurement over a range of 10^{11} to 10^{16} ions per square centimeter--this is an ion-implanted doping--we have a sensitivity of about a percent change in doping level. In some other experiments that were done in this SEM system, it appeared, but it wasn't really tested very well, that the sensitivity was a few percent. You could see a few percent change in the amount of doping that was in the material.

Mr. H. K. Wickramasinghe (IBM): Coming back to the experiment that you just described, do you fully understand the contrast mechanism in the doped images that you show?

Mr. Opsal: In the doped?

Mr. Wickramasinghe: Can you quantify the contrast?

Mr. Opsal: Now, let me see if I understand your question.

Mr. Wickramasinghe: How do you quantify the contrast that you see in the doped specimen? In other words, you go from 10^{11} to 10^{16}.

Mr. Opsal: Oh, I didn't show any pictures that showed doping variation over that range, but--yes, from other measurements where we are making a more direct measurement of the thermal wave itself, we think that dopant variations produce variations in the thermal conductivity which give rise to the contrast seen in some of the images of integrated circuits.